

Optical and thermal depth profile reconstructions of inhomogeneous photopolymerization in dental resins using photothermal waves

P. Martínez-Torres,^{1,a)} A. Mandelis,² and J. J. Alvarado-Gil¹

¹*Department of Applied Physics, CINVESTAV Unidad Mérida, Antigua Carretera a Progreso Km. 6, 97310 Mérida, Yucatán, Mexico*

²*Department of Mechanical and Industrial Engineering, Center for Advanced Diffusion-Wave Technologies, University of Toronto, 5 King's College Road, Toronto, Ontario M5S 3G8, Canada*

(Received 26 April 2010; accepted 8 July 2010; published online 3 September 2010)

Photopolymerization is a process that depends, among other factors, on the optical properties of polymerized materials. In turn, this process affects longitudinal light transport in these materials, thereby altering their optical absorption coefficient which is thus expected to exhibit depth dependence. Furthermore, polymerization affects the thermal properties of these materials. A robust theoretical approach to the study of the depth-dependent optical absorption coefficient, $\beta(x)$, and thermal diffusivity, $\alpha(x)$, in materials exhibiting depth profiles of these parameters has been developed through the photothermal inverse problem based on the concept of the thermal-harmonic oscillator. Using this concept in the frequency-domain nonhomogeneous photothermal-wave boundary-value problem, the simultaneous reconstruction of arbitrary simultaneous optical and thermal depth profiles was achieved using a multiparameter fitting method to the experimental amplitude and phase. As a first application of the theory to partially polymerized Alert Composite (shade A3) dental resin, with curing induced by a blue light-emitting diode, the $\beta(x)$ and $\alpha(x)$ depth profiles were reconstructed from photothermal radiometric frequency-scanned data. A strong anticorrelation of these two depth profiles was observed and was interpreted in terms of photochemical processes occurring during the optical (photocuring) creation of long polymeric chains in the resin. The photothermally reconstructed depth profiles may have implications for the optimization of blue light curing methods using such resins in dental clinical practice. © 2010 American Institute of Physics. [doi:10.1063/1.3475712]

I. INTRODUCTION

Dentistry is a field with rapid development of new products and materials. Characterization of dental materials for quality control is essential, especially if it can be done using nondestructive and noninvasive techniques. One important depth-profilometric technique that can be applied to evaluate these materials optically and thermally is photothermal (PT) radiometry (PTR). This technique belongs to the group of PT techniques that have been applied successfully to the nondestructive study of materials,¹⁻³ which are based on the generation of (photo) thermal waves in a sample. The rate of transport of conductive thermal energy by means of PT waves varies when they encounter inhomogeneities,⁴ making this type of techniques attractive for characterizing inhomogeneous materials.^{5,6}

Due to the importance of monitoring and evaluating inhomogeneous materials, PT techniques have been developed to probe depth-dependent thermal properties.^{6,7} Various mathematical approaches have been developed to reconstruct depth profiles of thermal properties from PT frequency-scanned experimental data.⁸⁻¹³ Some of those methods involve a judiciously structured functional form for the continuously variable depth-dependent inhomogeneous thermal properties (diffusivity or conductivity) and solving the thermal-wave differential equation boundary-value

problem.^{6,9,14} Another approach consists of virtually slicing a solid into a system of N-layers, each with constant thermal properties, and solving N-coupled differential thermal-wave equations with boundary conditions of temperature and heat flux.^{10,13,15} Also, several algorithms to invert the depth profiles have been applied, using an inverse procedure to find the Taylor expansion parameters of the conductivity profile,^{9,16} a least-squares one-parameter fit to reconstruct a polygonal approximation to the conductivity profile,^{17,18} obtaining local thermal diffusivity at each frequency,^{12,14,19} global optimization methods as genetic algorithm and neuronal networks,²⁰⁻²² and particle swarm optimization.¹³ Experimentally, some of these theories have been applied to evaluate liquid crystals,^{23,24} ceramics,²⁵ metallurgical specimens,^{17,26,27} aluminum oxide thin films,²² and dental resin composites,²⁸ to name a few. All these approaches concern only depth-dependent variations in the thermal parameters of materials while the optical properties remain either constant or the material is optically opaque (PT saturation).

Concurrently, much work has been done in the field of inverse problem theory in optical depth profilometry using several techniques based on optical absorption, photoluminescence, elastic, and inelastic scattering.⁸ Some reports have also been published on optical absorption depth profiles using PT techniques, in which the variation in the optical absorption coefficient is considered while keeping the thermal properties constant. The earliest theoretical work in this area was published by Afromowitz *et al.*²⁹ and Harata and

^{a)}Electronic mail: ptorres@mda.cinvestav.mx.

Sawada³⁰ introduced a simple approximation method for that theory. Schweitzer and Power³¹ have presented a theoretical and experimental study for depth profiling the optical absorptivity in thermally quasihomogeneous materials in which absorptivity varies arbitrarily with respect to the depth. Hodgson³² introduced standard regularization methods and procedures for the solution of the original theory of Afromowitz *et al.* A PT mathematical model for transient emission radiometric noninvasive measurements of the optical absorption depth profile of water concentration in human skin using a genetic algorithm was developed by Cui *et al.*²¹ In all those studies the thermal properties were independent of depth.

New dental resins are constantly being developed and improved with very promising physical properties that make them suitable for replacing amalgams. They have important advantages like good aesthetic characteristics and low cost, however, their mechanical and optical properties can be crucial factors in their clinical performance. In particular, photocurable resins are among the most versatile, due to the fact that they can be molded as needed and subsequently cured with a low power light source. However, it has been found that photocured composite resins exhibit a gradual decrease in microhardness with increasing depth^{33–35} as well as depth-dependent variations in their optical properties.^{36,37} This phenomenon is due to the fact that the curing light flux depends on the distance from the illuminated surface of the sample thereby generating partial polymerization of the monomers depthwise in the material.³⁸ For this reason, it is important to evaluate and characterize the degree of polymerization of photocured dental resins.

The conventional techniques used to evaluate mechanical and optical properties of polymerizable materials are hardness testing and UV-VIS optical spectroscopy, respectively. As mentioned above, PT techniques have the capability to measure the optical absorption or thermal depth profiles of a sample. Therefore, it is expected that they can also become suitable tools for simultaneously evaluating superposed optical and thermal depth profiles.

In this paper, a PT wave inverse theory using the concept of the Hamilton–Jacobi thermal-harmonic oscillator³⁹ is developed for the simultaneous reconstruction of optical and thermal depth profiles in solids. The theory is based on the extension of the earlier inverse problem approach to the reconstruction of thermal diffusivity or conductivity in optically opaque solids.⁶ The approach is proposing two functional forms describing the depth dependence of the optical absorption coefficient and the thermal diffusivity, followed by simultaneous reconstructions of these parameters by means of multiparameter fits of the experimental data at each frequency. The theory is applied to depth profile reconstructions of partially cured dental resins of Alert composite from experimental data obtained with PTR. The sample was partially cured by illuminating one side with a blue light-emitting diode (LED). After curing, the sample was illuminated from the opposite side with a modulated IR laser beam performing a PTR frequency scan and detecting the emitted back-scattered thermal IR radiation.

II. THEORY

A one-dimensional (1D) PT wave theoretical model is considered which takes into account inhomogeneous optical and thermal properties. In this case, the thermal-wave-field for a semi-infinite medium with continuously variable thermal conductivity, $k(x)$, density, $\rho(x)$, and specific heat, $c(x)$, is given by the solution of the heat conduction equation

$$\frac{\partial}{\partial x} \left[k(x) \frac{\partial}{\partial x} \Theta(x, t) \right] - \rho(x)c(x) \frac{\partial}{\partial t} \Theta(x, t) = -Q(x)(1 + e^{i\omega t}); \quad x \geq 0, \quad (1)$$

where $Q(x)(1 + e^{i\omega t})$ is the spatially-dependent harmonic source function and ω is the angular modulation frequency of the heat source. Under harmonic optical excitation, $\Theta(x, t) = T(x)e^{i\omega t}$, Eq. (1) becomes

$$\frac{d}{dx} \left[k(x) \frac{d}{dx} T(x) \right] - i\omega\rho(x)c(x)T(x) = -Q(x); \quad x \geq 0, \quad (2)$$

The homogeneous temperature field solution of Eq. (2) is given by⁶

$$T_h(x) = \sqrt{\frac{e_0}{e_s(x)}} [c_1 e^{H(x)} - c_2 e^{-H(x)}], \quad (3)$$

with

$$H(x) = \int_0^x \sigma(y) dy = \int_0^x \sqrt{\frac{i\omega}{\alpha_s(y)}} dy, \quad (4)$$

where $\alpha_s(x) = k(x)/\rho(x)c(x)$ and $e_s(x) = \sqrt{k(x)\rho(x)c(x)}$ are the material thermal diffusivity and effusivity, respectively. e_0 is the material thermal effusivity at $x=0$; c_1 and c_2 are integration constants to be determined from boundary conditions. The conditions for the validity of this solution, akin to the Wentzel–Kramers–Brillouin–Jeffreys approximation, assume⁶ negligible contribution to the temperature profile from a term proportional to the spatial rate of change in the inverse square root of the thermal effusivity $e_s(x)$. This condition is well satisfied in all cases where the rate of change in thermal conductivity and/or diffusivity is a continuous function of depth and not sudden (a step-function). This is also the case in the present applications (see Appendix).

Following Ref. 6, we assume a particular solution of Eq. (2) of the form

$$T_p(x) = \sqrt{\frac{e_0}{e_s(x)}} [P(x)e^{H(x)} - G(x)e^{-H(x)}], \quad (5)$$

where $e_0 \equiv e_s(0)$. Then applying the method of variation in parameters, subject to $(dP(x)/dx)e^{H(x)} + (dG(x)/dx)e^{-H(x)} = 0$, and making the approximation

$$\frac{d}{dx} e_s^{-1/2}(x) \approx 0, \quad 0 \leq x < \infty, \quad (6)$$

after some manipulation, it can be shown that for semi-infinite solids

$$P(x) = -\frac{1}{2} \int_0^x Q(y) e^{-H(y)} \frac{E^{1/2}(y)}{k(y)\sigma(y)} dy, \quad (7a)$$

$$G(x) = \frac{1}{2} \int_0^x Q(y) e^{H(y)} \frac{E^{1/2}(y)}{k(y)\sigma(y)} dy, \quad (7b)$$

where $E(x) = e_s(x)/e_0$. From Eqs. (3), (5), and (7), assuming a finite optical absorption coefficient β so that $Q = Q(x, \beta)$ the complete solution for the inhomogeneous PT wave is given by

$$T(x, \beta) = \left[c_1 - \frac{1}{2} \int_0^x Q(y, \beta) e^{-H(y)} \frac{E^{1/2}(y)}{k(y)\sigma(y)} dy \right] \frac{e^{H(x)}}{E^{1/2}(x)} - \left[c_2 - \frac{1}{2} \int_0^x Q(y, \beta) e^{H(y)} \frac{E^{1/2}(y)}{k(y)\sigma(y)} dy \right] \frac{e^{-H(x)}}{E^{1/2}(x)}. \quad (8)$$

Now, imposing the boundary conditions

$$(i) \quad T(x \rightarrow \infty, \beta) = 0,$$

$$(ii) \quad k(0) \frac{d}{dx} T(x, \beta) \Big|_{x=0} = AT(0, \beta),$$

here A is the radiation heat transfer coefficient ($\text{W cm}^{-2} \text{K}^{-1}$) at $x=0$ at the nonhomogeneous solid—air interface. The constants c_1 and c_2 are

$$c_1 = \frac{1}{2} \int_0^\infty Q(y, \beta) e^{-H(y)} \frac{E^{1/2}(y)}{k(y)\sigma(y)} dy, \quad (9a)$$

$$c_2 = -\left(\frac{k_i \sigma_i - A}{k_i \sigma_i + A} \right) c_1, \quad (9b)$$

substituting Eqs. (9) in Eq. (8), the thermal wave-field for the semi-infinite inhomogeneous solid becomes

$$T(x, \beta) = \frac{1}{2} \left\{ \left[- \int_\infty^x Q(y, \beta) e^{-H(y)} \frac{E^{1/2}(y)}{k(y)\sigma(y)} dy \right] \frac{e^{H(x)}}{E^{1/2}(x)} + \left[\left(\frac{k_i \sigma_i - A}{k_i \sigma_i + A} \right) \int_0^\infty Q(y, \beta) e^{-H(y)} \frac{E^{1/2}(y)}{k(y)\sigma(y)} dy + \int_0^x Q(y, \beta) e^{H(y)} \frac{E^{1/2}(y)}{k(y)\sigma(y)} dy \right] \frac{e^{-H(x)}}{E^{1/2}(x)} \right\}. \quad (10)$$

It can be seen that when $Q(x, \beta) = Q_0 \beta e^{-\beta x}$, Eq. (8) reduces to the expression given by Mandelis *et al.*⁶ for the case of solids with constant and finite optical absorption coefficient β and continuously inhomogeneous thermal properties.

From Eq. (10), the PT wave-field at $x=0$ is given by

$$T(0, \beta) = \left(\frac{k_i \sigma_i}{k_i \sigma_i + A} \right) \int_0^\infty Q(y, \beta) e^{-H(y)} \frac{E^{1/2}(y)}{k(y)\sigma(y)} dy = \left(\frac{1}{k_i \sigma_i + A} \right) \int_0^\infty \frac{Q(y, \beta) e^{-H(y)}}{E^{1/2}(y)} dy. \quad (11)$$

Equation (11) will be solved by assuming a particular functional form for inhomogeneous optical and thermal varia-

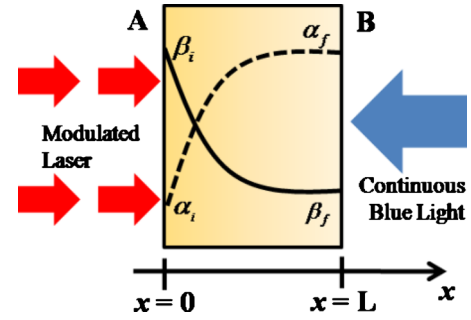


FIG. 1. (Color online) An optically and thermally nonhomogeneous solid (a dental filling material) with arbitrary optical absorption coefficient and thermal diffusivity depth profiles generated through illumination with a blue curing light.

tions inside the semi-infinite solid (Fig. 1). For the optical absorption coefficient variation a simple *ad hoc* mathematical functional form is

$$\beta(x) = \beta_i \left(\frac{1 + \delta e^{-gx}}{1 + \delta} \right), \quad (12)$$

where, at $x=0$ the optical absorption coefficient is β_i and $\beta(\infty) = \beta_f$, with $\beta_i > \beta_f$ and $\delta = (\beta_i/\beta_f) - 1$. g is a parameter that will be determined from the experimental data and determines the spatial rate of decrease in the optical absorption coefficient. It will be noticed that the profile of Eq. (12) is flexible enough to allow for a depthwise increase in $\beta(x)$ with $\beta_i < \beta_f$ which renders $\delta < 0$. At the same time, an inhomogeneous thermal diffusivity profile is considered⁶

$$\alpha_s(x) = \alpha_i \left(\frac{1 - \Delta e^{-qx}}{1 - \Delta} \right)^2 \quad \text{with} \quad \Delta \equiv 1 - \left(\frac{\alpha_i}{\alpha_f} \right)^{1/2}, \quad (13)$$

where $\alpha_s(0) = \alpha_i$ and $\alpha_s(\infty) = \alpha_f$, with $\alpha_i < \alpha_f$. q is a constant that determines the spatial rate of thermal diffusivity growth (or decay, if $\alpha_i > \alpha_f$). In summary, Eqs. (12) and (13) are very flexible universal expressions because their parameters can vary with frequency, thus adapting the profile to changing local values of thermal diffusivity and optical absorption coefficient consistent with the experimental data (PT amplitude and phase) at that frequency.

In order to obtain the function $Q(x, \beta)$ to be substituted in Eq. (11), a variation in propagating light intensity according to the Beer-Lambert law will be assumed

$$\frac{dI(x)}{dx} = -\beta(x)I(x). \quad (14)$$

Substituting Eq. (12) into Eq. (14) and integrating yields

$$I(x) = I_0 \exp \left[-\beta_f \left(x - \frac{\delta}{g} e^{-gx} \right) \right] + \text{constant}, \quad (15)$$

so that

$$Q(x, \beta) = -\frac{dI}{dx} = \frac{1}{2} I_0 \beta_f (1 + \delta e^{-gx}) \exp \left[-\beta_f \left(x - \frac{\delta}{g} e^{-gx} \right) \right], \quad (16)$$

$I_0 \equiv I(0)$ is the amplitude of the modulated optical intensity incident on the sample surface. Using the expansion e^x

$=\sum_{n=0}^{\infty}(x^n/n!)$ for the last term of Eq. (16), $Q(x, \beta)$ can be written as

$$Q(x, \beta) \approx I_0 \beta_f (1 + \delta e^{-gx}) \sum_{n=0}^{\infty} \left(\frac{R^n}{n!} \right) e^{-(\beta_f + ng)x}, \quad (17)$$

with $R = (\delta/g)\beta_f$. If $\beta_i - \beta_f < g$ then $R < 1$, and this series can be truncated.

Additionally, substituting Eq. (13) into Eq. (4) yields

$$H(x) = \sigma_f x + \ln \left(\frac{1 - \Delta e^{-qx}}{1 - \Delta} \right)^{\sigma_f/q}. \quad (18)$$

Assuming that $E(x) \approx [\alpha_s(x)/\alpha_i]^{1/2}$ (i.e., $\rho c \sim \text{constant}$ across the solid) and substituting Eqs. (17) and (18) into Eq. (11)

$$T(0, \beta) = \left(\frac{I_0 \beta_f}{k_i \sigma_i + A} \right) \sum_{n=0}^{\infty} \frac{R^n}{n!} \int_0^{\infty} \left(1 + \delta e^{-gy} \right) e^{-(\beta_f + \sigma_f + ng)y} \left(\frac{1 - \Delta e^{-qy}}{1 - \Delta} \right)^{-(\sigma_f/q + 1/2)} dy, \quad (19)$$

making the change in variable $u = e^{-qx}$,

$$T(0, \beta) = \left(\frac{I_0 \beta_f}{k_i \sigma_i + A} \right) \frac{(1 - \Delta)^L}{q} \sum_{n=0}^{\infty} \frac{R^n}{n!} \left[\int_0^1 u^{K_n} (1 - \Delta u)^{-L} du + \delta \int_0^1 u^{G_n} (1 - \Delta u)^{-L} du \right], \quad (20)$$

with $L \equiv (\sigma_f/q) + (1/2)$, $K_n \equiv (\beta_f + \sigma_f + ng/q) - 1$, and $G_n \equiv [\beta_f + \sigma_f + (n+1)g/q] - 1$.

In Eq. (20) the integrals inside the parentheses can be represented in terms of the confluent hypergeometric function⁴⁰

$$F(\alpha, \beta; \gamma; z) = \frac{1}{B(\beta, \gamma - \beta)} \int_0^1 t^{\beta-1} (1-t)^{\gamma-\beta-1} (1-tz)^{-\alpha} dt; \quad \text{Re } \gamma > \text{Re } \beta > 0;$$

with $B(x, y) = \int_0^1 t^{x-1} (1-t)^{y-1} dt$ the definition of the Beta function (Euler's integral of the first kind). Therefore, Eq. (20) can be written as

$$T(0, \beta) = \left(\frac{I_0 \beta_f}{k_i \sigma_i + A} \right) \frac{(1 - \Delta)^L}{q} \sum_{n=0}^{\infty} \frac{R^n}{n!} \left[\frac{F(L, K_n + 1; K_n + 2; \Delta)}{K_n + 1} + \delta \frac{F(L, G_n + 1; G_n + 2; \Delta)}{G_n + 1} \right]. \quad (21)$$

It is noted that when $\Delta < 1$, the hypergeometric function can be expressed in terms of the series⁴⁰

$$F(a, b; c; z) = \frac{\Gamma(c)}{\Gamma(a)\Gamma(b)} \sum_{m=0}^{\infty} \frac{\Gamma(a+m)\Gamma(b+m)}{m!\Gamma(c+m)} z^m. \quad (22)$$

The PT wave-field for a semi-infinite material with homogeneous thermal properties that corresponds to the dental material *before curing* is given by

$$T_{\text{homogeneous}}(0, \beta_i) = \frac{I_0 \beta_i}{2(\beta_i + \sigma_i)(k_i \sigma_i + H)}, \quad (23)$$

where H is the radiation heat transfer coefficient ($\text{W cm}^{-2} \text{K}^{-1}$) at $x=0$ for the sample before curing. Equation (21) must be normalized by Eq. (23) so as to avoid introducing the instrumental transfer function in the frequency response of the nonhomogeneous solid,

$$T_N(x=0) = \frac{2\rho\beta_f(\sigma_i + h)}{\beta_i(\sigma_i + a)} \frac{(\beta_i + \sigma_i)(1 - \Delta)^L}{q} \sum_{n=0}^{\infty} \frac{R^n}{n!} \left[\frac{F(L, K_n + 1; K_n + 2; \Delta)}{K_n + 1} + \delta \frac{F(L, G_n + 1; G_n + 2; \Delta)}{G_n + 1} \right], \quad (24)$$

where $a = A/k_i$ and $h = H/k_i$. The parameter ρ is a scaling constant from the normalization that is related with the emissivity and reflectivity of the sample before and after curing.

III. MATERIALS AND METHODS

The experimental PTR system for performing frequency scans of photopolymerized dental resin samples is shown in

Fig. 2. A high-power (20 W) IR laser (Jenoptik JOLD-X-CPXL-1L, 808 nm) was current modulated at a frequency f , using a ThorLabs high-power laser driver. The laser beam was focused directly onto the surface of the sample (1 cm diameter). This spot size allows generating 1D PT waves, thereby simplifying the theoretical and computational analyses by avoiding complications due to lateral heat diffusion.^{41,42} The IR radiation from the optically excited

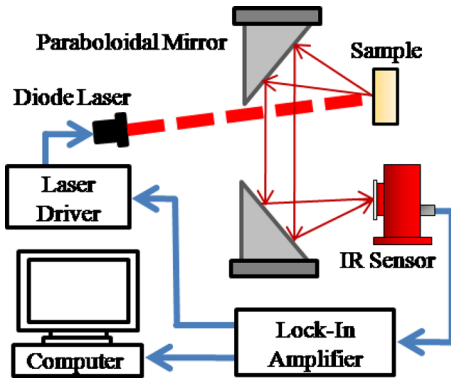


FIG. 2. (Color online) Schematic view of the PTR experimental setup.

sample surface was collected and collimated by two silver-coated, off-axis paraboloidal mirrors, and then focused onto a liquid-nitrogen-cooled HgCdTe (mercury–cadmium–telluride) detector (EG&G Judson J15D12-M204-S01M-60-WE). The heated area of the sample was at the focal point of one mirror and the detector was at the focal point of the other mirror. The detector had an active area of 1 mm^2 and spectral bandwidth of $2\text{--}12 \text{ }\mu\text{m}$. An antireflection-coated germanium window with a transmission bandwidth of $2\text{--}14 \text{ }\mu\text{m}$ was mounted in front of the detector to block any radiation from the laser. The PTR signal was amplified by a low-noise preamplifier (EG&G Judson PA101) and sent to the digital lock-in amplifier (SR830). The lock-in amplifier received and demodulated the preamplifier output, amplitude, and phase of the PTR signal, which were recorded as functions of frequency in a personal computer.

The commercial dental resin Alert condensable composite (shade A3) manufactured by Pentrol Clinical Technologies, LLC, was used to obtain optical absorption and thermal diffusivity depth profiles. Each resin composite sample was formed into a cylindrical-disk of 1 cm diameter and 2 mm height (thermally semi-infinite). A glass slide was placed on both surfaces of the disk and gentle pressure was applied to extrude excess material and produce a flat surface. The glass slides were withdrawn and the sample was mounted on the

PTR system to obtain the optical and thermal profiles in the back-propagation emission configuration. First, a frequency scan of the sample before curing in the range $1.5\text{--}1000 \text{ Hz}$ was performed. Next, partial polymerization of the dental resin was induced by illuminating the sample on one side for one minute with a 30 mW/cm^2 light using a high-power blue LED (457 nm). The LED light was partially absorbed longitudinally along the resin bulk, generating gradual depth-dependent polymerization of the sample. To generate PT signals, the opposite side of the sample was illuminated with the probe laser and the radiation emitted from that surface was collimated and collected with the mirrors and sent into the IR detector (see Fig. 1). Following the curing process, a new frequency scan of the partially polymerized sample was performed in the same frequency range. It must be mentioned that one of the principal assumptions is that the sample is opaque to the IR radiation in the spectral detection range of HgCdTe sensor,^{43–45} so that the main contribution to the PTR signal comes from the changes in temperature on the surface of the resin sample [see Eq. (25)].

IV. RESULTS AND DISCUSSION

Figures 3(a) and 3(b) show the PTR signal amplitude and phase, respectively, from a typical dental resin sample before and after partial curing, measured in the back-propagated emission configuration. The curing imparted thermal and optical depthwise inhomogeneities to the resin. As discussed above, direct normalization of amplitude (ratio) and phase (difference) of the partially cured sample was performed with respect to the sample before curing. From visual inspection it was observed that before curing the sample surface was smooth and the dental resin density in the sample holder was uniform.

Before normalizing, each curve was smoothed with an eleventh degree polynomial in order to minimize the well-known effects of noise and random errors in the PT depth-profilometric reconstructions.^{6,19,23} Using this smoothing fit, a set of 500 points was generated over the experimental frequency range. Figure 4 shows the PTR signal amplitude and

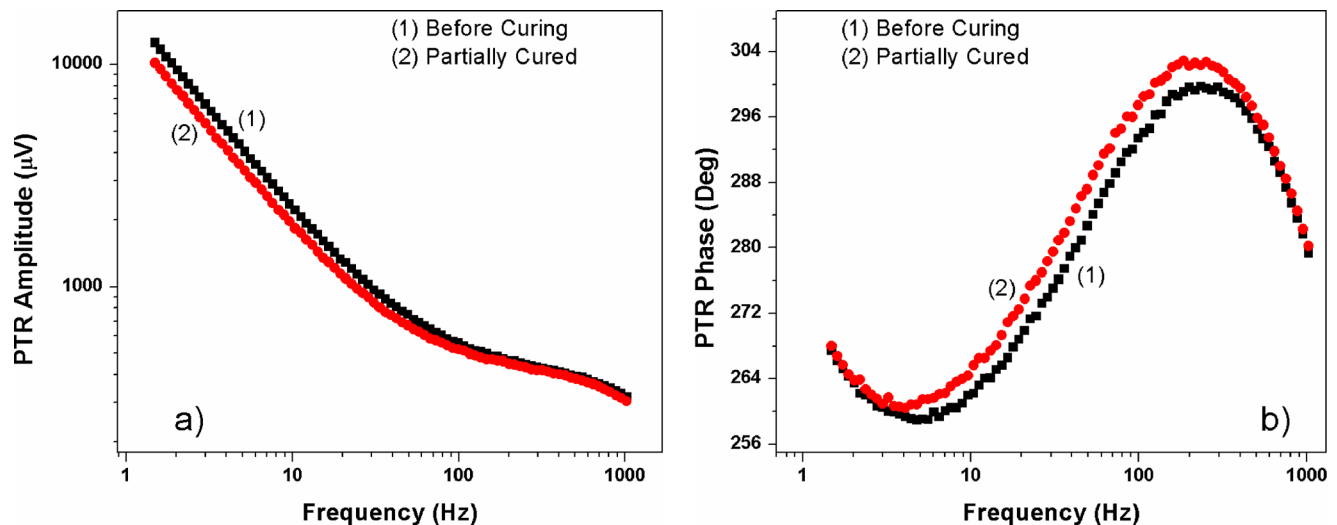


FIG. 3. (Color online) (a) PTR amplitude and (b) PTR phase signals from the dental resin before and after partial curing.

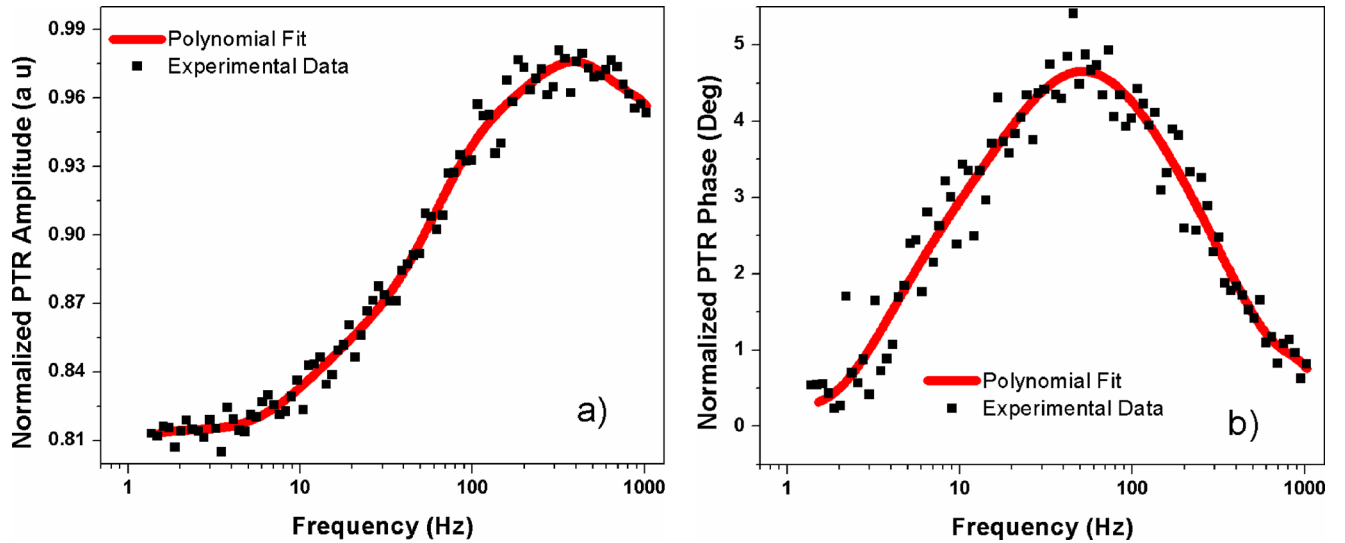


FIG. 4. (Color online) Normalized PTR signal for a typical partially cured sample. (a) Amplitude ratio and (b) phase difference.

phase of the partially cured sample normalized with respect to the PTR signal before curing. Variations in amplitude ratio and phase difference with frequency are related to the variations in the optical absorption coefficient and thermal diffusivity with depth due to the inhomogeneous degree of polymerization in the sample.

The first step was to obtain values of all the parameters by applying a multiparameter fit to the experimental data with the objective to determine the parameters that are going to be kept constant during the depth-profilometric reconstruction. Then, the reconstruction process started by finding the local optical absorption and thermal diffusivity for each frequency. Experimentally the PTR signal was measured in amplitude and phase. The normalized Eq. (24) can be written as $|M(\omega)|e^{i\Delta\phi(\omega)}$, where $|M(\omega)|$ and $\Delta\phi(\omega)$ are the amplitude ratio and phase difference at angular frequency ω .

The PT wave-field $T(x, \beta, \alpha_s, \omega)$ generates the overall Planck radiation emission signal integrated over the depth of the sample

$$S(\beta, \alpha_s, \omega) \propto \beta_{\text{IR}} \int_0^{\infty} e^{-\beta_{\text{IR}}x} T(x, \beta, \alpha_s, \omega) dx, \quad (25)$$

β_{IR} is the spectral averaged effective infrared absorption/emission of the medium. Taking into account that the dental resin composite is a polymeric material that has several strong IR absorption bands in the spectral detection range of the HgCdTe sensor for the cured and uncured material,⁴³⁻⁴⁵ it is assumed that $\beta_{\text{IR}} \gg \beta$. In this case, an approximation can be made as follows:⁴⁶ $\lim_{\beta_{\text{IR}} \rightarrow \infty} (\beta_{\text{IR}} e^{-\beta_{\text{IR}}x}) = \delta(x)$, and Eq. (25)

gives

$$\begin{aligned} S(\beta, \alpha_s, \omega) &\propto \beta_{\text{IR}} \int_0^{\infty} e^{-\beta_{\text{IR}}x} T(x, \beta, \alpha_s, \omega) dx \\ &\rightarrow \int_0^{\infty} \delta(x) T(x, \beta, \alpha_s, \omega) dx \rightarrow T(0, \beta, \alpha_s, \omega), \end{aligned}$$

therefore, the main contribution to the PTR signal comes from the changes in temperature on the surface of the dental

resin sample. This justifies the validity of Eqs. (21), (23), and (24) that will be used in the inversion procedure.

Given that the analytical separation of Eq. (24) in magnitude and phase is a rather difficult or even impossible process, a numerical solution was obtained. The minimum number of terms sufficient to represent the infinite series in Eq. (24) was determined by a simulation, starting with the n th term of the optical absorption coefficient profile expansion and one for each of the two hypergeometric functions in the summand. That simulation was compared with the $(n+1)$ th term simulation for both expansion series, and so on. As a general rule, after three terms of the series expansion, no measurable change was observed in the simulations.

Due to the fact that the PTR signal has two channels (amplitude and phase), each with complementary information about the material parameters, both channels had to be taken into account during the multiparameter fits. The way to satisfy the foregoing condition is through defining the combined error at each frequency as

$$\begin{aligned} \chi_j^2 &= [M_{\text{exp}}(\omega_j) - M_{\text{theory}}(\omega_j)]^2 + [\Delta\phi_{\text{exp}}(\omega_j) \\ &\quad - \Delta\phi_{\text{theory}}(\omega_j)]^2, \end{aligned} \quad (26)$$

where the total error is

$$\chi^2 = \sum_{j=1}^n \chi_j^2; \quad (27)$$

n is the number of frequency scan points.

Once the minimum number of terms sufficient to represent the infinite series of the PT wave-field given by Eq. (24) was determined numerically, it was possible to use our multiparameter fitting algorithm as described below and find the parameters ρ , a , h , β_i , β_f , α_i , α_f , g , and q which best-fitted that equation to the normalized experimental data, Fig. 4. The major problem of using a multiparameter fitting procedure is lack of uniqueness of the solution due to multiple combinations of parameters that could fit the experimental data with good fidelity. The constraint is that all parameters must be real and positive quantities and that they should be

physically acceptable, i.e., the values should be within a range based on known literature values was applied and proved to be an excellent uniqueness criterion. The Downhill Simplex method was used⁴⁷ to fit the PTR experimental data through minimizing χ^2 , subject to the aforementioned constraint: Selection of the initial parameters within a range based on literature values. Additionally, $\beta_i - \beta_f < g$ was applied to retain the validity of the approximation made in Eq. (17), where $\beta_i > \beta_f$. This assumption was introduced from visual inspection which showed photobleaching after photopolymerization. Furthermore, we set the constraint $\alpha_i < \alpha_f$ because the value of the bulk thermal diffusivity for a similar resin after curing²⁸ is known to increase. A similar trend was recently observed in the bulk thermal diffusivity value of the present resin, as measured with an opaque thin metallic coating on the surface leading to purely thermal diffusivity reconstruction without the (photothermally saturated) optical absorption coefficient.²⁸ Reasonably assuming that all changes in PTR signal after photopolymerization are due to inhomogeneities of the optical and thermal properties of the sample, arbitrary depth profiles for the optical absorption and thermal diffusivity can be reconstructed by numerically determining the optimal pair of (β_f, g) and (α_f, q) at each angular frequency, so that the assumed profile locally results in the experimentally observed PT wave signal amplitude and phase data.

Once the starting values of ρ , a , h , β_i , β_f , α_i , α_f , g , and q were determined from the first step, the second step was to find local values of $[\beta_{f(j)}, g_{(j)}]$ and $[\alpha_{f(j)}, q_{(j)}]$, fix the previously calculated parameters ρ , a , h , β_i , α_i , and apply the Downhill Simplex method to minimize the χ_j^2 at each frequency subject to the constraints that $\beta_i - \beta_{f(j)} < g_{(j)}$ with $\beta_i > \beta_{f(j)}$ and $\alpha_i < \alpha_{f(j)}$. When the entire set of local values of $[\beta_{f(j)}, g_{(j)}]$ and $[\alpha_{f(j)}, q_{(j)}]$ became known, the thermal diffusivity and optical absorption coefficient depth profiles of the sample were calculated. The calculation for reconstructing the depth parameter x_j was performed based on the fact that, as the modulation frequency decreases, the thermal-wave probe depth increases. Starting at the highest angular frequency, ω_0 , the shortest depth, x_0 , is the shortest thermal diffusion length, i.e., $x_0 = (2\alpha_0/\omega_0)^{1/2}$, the next lower frequency x_{j+1} corresponds to an increased thermal-wave depth

$$x_{j+1} = x_j + \sqrt{\frac{2\alpha_{s(j)}}{\omega_{j+1}}} - \sqrt{\frac{2\alpha_{s(j)}}{\omega_j}}, \quad (28)$$

which is then substituted into Eq. (13) to calculate $\alpha_{s(j+1)}$. Once $\alpha_{s(j+1)}$ is calculated the method returns to recursively revise and improve the accuracy of the thermal-wave virtual depth slice as

$$x_{j+1} = x_j + \sqrt{\frac{2\alpha_{s(j+1)}}{\omega_{j+1}}} - \sqrt{\frac{2\alpha_{s(j)}}{\omega_j}}. \quad (29)$$

Therefore, the depth of each virtual slice depends on ω_j and $\alpha_{s(j)}$. Then, each x_j is substituted into Eq. (12) to calculate $\beta_{s(j)}$. Thus, the depth profiles for the thermal diffusivity and optical absorption coefficient are built up by individual consecutive slice profiles.

Figure 5 shows the reconstructed thermal diffusivity and optical absorption depth profiles for four samples prepared and measured under the same conditions of photopolymerized dental resin composites (2 mm thick) in the back-emission configuration applying the foregoing theory and computational multiparameter algorithm. It can be seen that the thermal diffusivity profiles increase within the first 60 μm , followed by a smooth variation until a bulk thermal diffusivity value is attained. Regarding independent validation of the depth profiles, although mechanical hardness measurements were not performed in the studies reported in this paper, the present thermal diffusivity depth profiles are similar in rate of increase and saturation depth to those obtained earlier on the same samples with a thin opaque coating on the surface and single-parameter reconstruction.²⁸ These facts point to the robustness of the inversion methodology. The simultaneously reconstructed optical absorption coefficient profiles show good anticorrelation with the thermal diffusivity profiles consisting of a steep decrease in the first 60 μm followed by a slower decrease up to a final optical absorption value. The trends and values of the optical absorption coefficient depth profiles are in agreement with bulk absorption coefficients reported for similar dental resins measured in the range of UV-VIS wavelengths.^{30,37,48} Optical transmittance was used to verify the values of the reconstructed optical absorption coefficients at 808 nm. The ratio between the sample optical absorption coefficient before and after curing was (2.0 ± 0.2) .

In addition, by performing reconstructions varying the input parameters of thermal diffusivity and optical absorption coefficient before curing according to the upper and lower limits of the experimental errors, it was determined that our thermal diffusivity and optical absorption coefficient reconstructions exhibit an error smaller than 5% and 10%, respectively. An additional source of error comes from random noise variations in the magnitude and phase from point to point which can lead to fluctuations in the local estimates of the thermal diffusivity and optical absorption coefficient. This error was minimized by performing a fitting of the normalized data and interpolating to 500 points.

It is important to mention that those previous studies did not consider depth changes in optical absorption coefficients; they just provided the bulk (or possibly mean) optical absorption coefficients of the samples. Also, prior thermal-wave depth-profilometric studies have only considered the determination of either the optical absorption coefficient or the thermal diffusivity depth profiles but not the simultaneous reconstruction of both parameters. Therefore, the present double reconstruction methodology opens new possibilities for doing simultaneous depth reconstruction of optical and thermal properties using a unique set of measurements obtained by PT techniques.

Scattering in dental resins can be an important factor. However, based on computer simulations using the full diffuse photon density wave,⁴⁹ it was found that for thin samples a good first order approximation neglecting scattering is acceptable. In this sense, the optical absorption coefficient obtained from the reconstruction process must be considered as an effective optical absorption coefficient.

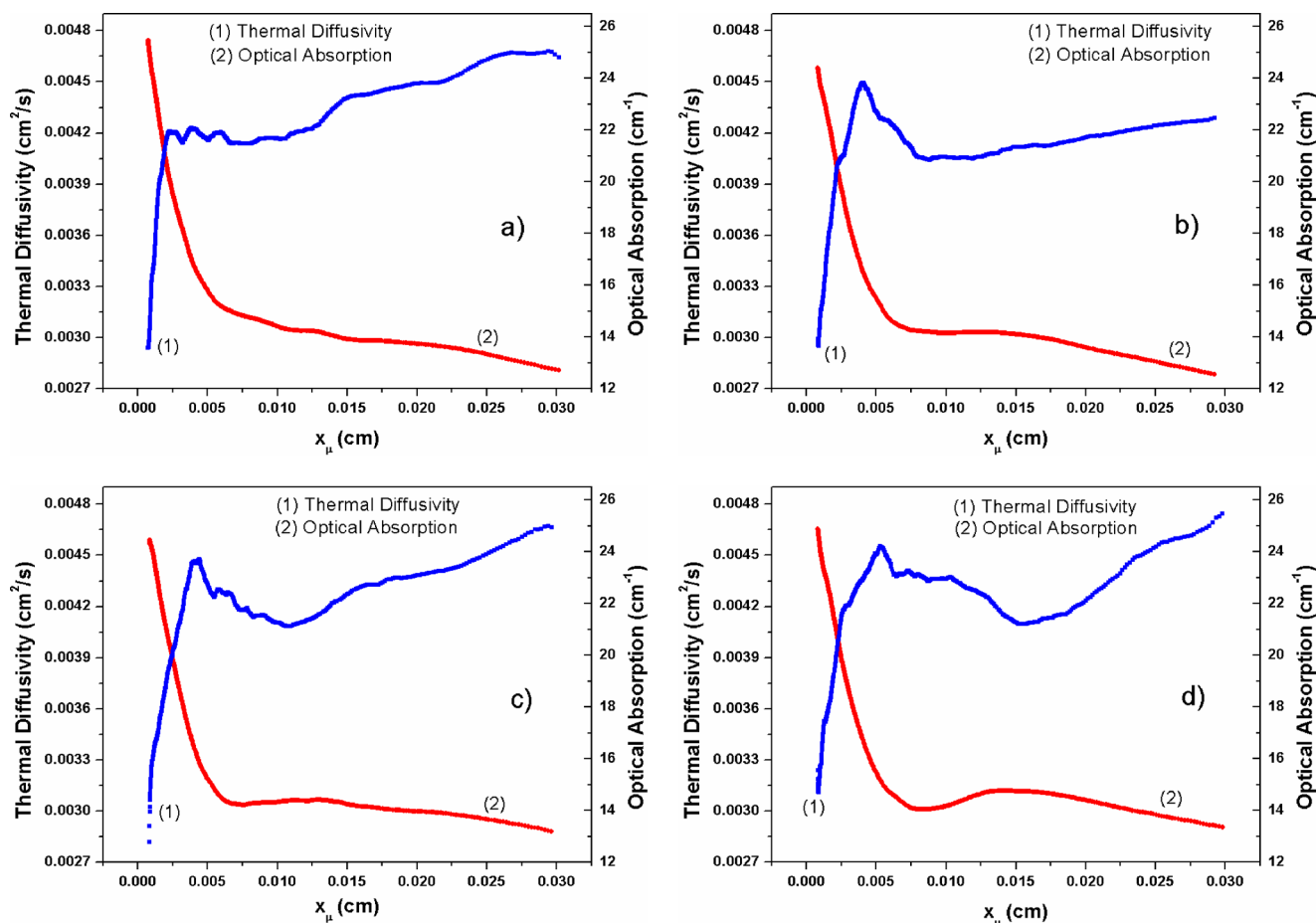


FIG. 5. (Color online) Thermal diffusivity and optical absorption depth profiles for four partially cured dental resin samples. x_μ is the reconstructed thermal-wave diffusion length at each modulation frequency. Curing occurred via illumination from side B of the sample (see Fig. 1).

Physically, the optical and thermal depth profiles across the sample are due to the fact that an incomplete (i.e., non-uniform) monomer-to-polymer conversion occurs during the surface illumination, because the curing blue light suffers optical attenuation as it propagates in the photopolymerizable material.^{50,51} This attenuation induces a partial polymerization that changes as a function of depth.^{38,52} It is expected that once the photopolymerization has started, the material exhibits a curing gradient with respect to the applied curing light (Fig. 1). The layer closer to the surface where the blue light was applied (side B) has a higher degree of conversion than the opposite surface (side A). This curing gradient is responsible for optical and thermal depthwise inhomogeneities in dental resins. The thermal diffusivity increase from $x=0$ (surface A) to $x=L$ (surface B) as reconstructed in Fig. 5 occurs because light curing promotes the growth of bonded chains in the dental resin, thereby enhancing heat diffusion along the polymer network away from the surface (B) where the blue light was applied.⁵³ In the case of the reconstructed optical absorption coefficient the reverse behavior is observed. This trend is related to the blue light-induced decomposition of the photoinitiator contained in the resin which, in turn, induces bond-chain formation. The direct consequence of the consumption of the photoinitiator is the assembly of long polymeric chains with lower optical absorption coefficient in the visible range of the electromagnetic spectrum.⁵⁴

Due to the gradual attenuation of the curing blue light along the material, it was shown that the reconstructed thermal and optical properties vary smoothly, i.e., without major abrupt variations amounting to discontinuities. Furthermore, the thermophysical field was evaluated at small incremental virtual depth slices, thus ensuring the absence of local steep thermal diffusivity gradients which would invalidate the solution approximation, Eq. (3), and guaranteeing the validity of the approximation given by Eq. (6) (Appendix).

V. CONCLUSIONS

This work has introduced a robust theoretical and computational methodology with multiparameter best fits at each frequency for the simultaneous reconstruction of optical and thermal depth profiles (optical absorption coefficient and thermal diffusivity) in inhomogeneous solids using PT waves with first application to the photopolymerization of dental resins partially cured by blue light. It has also been shown that PTR is a diagnostic PT technique highly suitable for the generation of these depth profiles as a result of dental resin curing. For the first time this novel approach allows a complete optothermal subsurface evaluation ($x < 300 \mu\text{m}$) of the effects of incomplete blue light curing of dental resins. The reconstructed thermal diffusivity profiles exhibit rapid increase within the first $60 \mu\text{m}$ followed by a slower and

smoother decrease toward a bulk thermal diffusivity value in agreement with literature data obtained under the assumption of constant diffusivity values. Similarly, the optical absorption coefficient profiles show good anticorrelation with the diffusivity depth profiles attaining bulk values in agreement with reports in the literature. A major insight of the present PT parameter reconstruction is the strong anticorrelation between optical absorption coefficient and thermal diffusivity depth profiles, Fig. 5, owing to the optical creation of long polymeric chains with decreased absorption coefficient and increased thermal diffusivity compared to the noncured dental resin. This may have implications for the optimization of blue light curing methods of such resins in dental clinical practice.

ACKNOWLEDGMENTS

This work was partially funded by the Multidisciplinary CINVESTAV Project 2009 and CONACyT Becas Mixtas program. The support of the Ministry of Research and Innovation (MRI) of Ontario in the form of the 2007 (inaugural) Premier's Discovery Award in Science and Engineering to A.M. is gratefully acknowledged.

APPENDIX

Equation (3) is an approximate solution to Eq. (2) assuming negligible contribution to the temperature profile from a term proportional to the spatial rate of change in the inverse square root of the thermal diffusivity,^{6,23} $e_s(x)$. Specifically, the heat flux at any depth x is

$$F(x) = -k(x) \frac{d}{dx} T(x). \quad (\text{A1})$$

Making use of Eq. (3)

$$F(x) = -k(x) e_0^{1/2} \left[\sigma(x) e_s^{-1/2}(x) + \left(\frac{d}{dx} e_s^{-1/2}(x) \right) \right] (c_1 e^{H(x)} - c_2 e^{-H(x)}), \quad (\text{A2})$$

This equation holds if

$$\frac{d e_s^{-1/2}(x)}{dx} \ll |\sigma_s(x)| e_s^{-1/2}(x). \quad (\text{A3})$$

Using the increasing $\alpha_s(x)$ profile [Eq. (13)] and the relationship $e_s(x) \approx \sqrt{\rho c \alpha_s(x)}$, where it is assumed that ρc does not change significantly before and after blue light curing, Eq. (A3) can be expressed as

$$\left(\frac{\omega}{\alpha_f} \right)^{1/2} \gg 2q\Delta e^{-qx}. \quad (\text{A4})$$

Using the values of $[\alpha_{f(j)}, q_{(j)}]$ obtained computationally in the derivation of our depth profiles, relation (A4) can be written as

$$F_1(\omega_j) \gg F_2[x_{\mu(j)}] \quad (\text{A5})$$

with

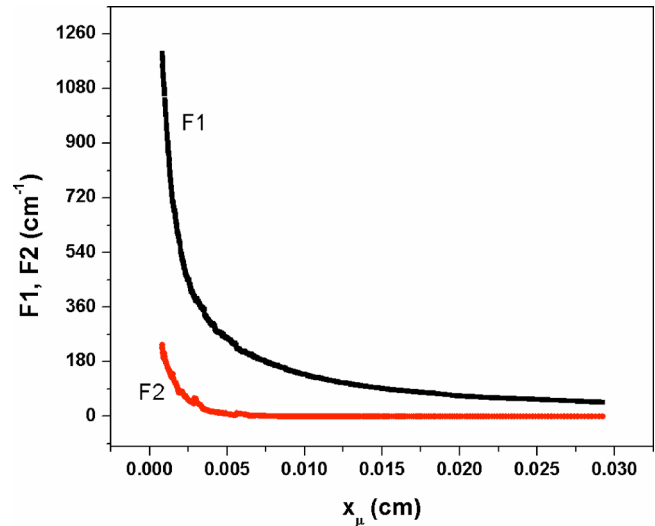


FIG. 6. (Color online) Comparison of magnitudes of $F_1(\omega)$ and $F_2(x)$ for one of the optical and thermal depth profile samples shown in Fig. 5.

$$F_1(\omega_j) = \left[\frac{\omega_j}{\alpha_{f(j)}} \right]^{1/2} \quad \text{and} \quad F_2[x_{\mu(j)}] = 2q_j \Delta_j e^{-q_j x_{\mu(j)}}.$$

Figure 6 shows the comparison of magnitudes F_1 and F_2 using the thermal parameters obtained for the thermal diffusivity depth profile of the sample shown in Fig. 5. Similar behavior is obtained for the other three samples. Therefore, it can be observed that condition (A5) is fulfilled satisfactorily.

¹D. Almond and P. Patel, *Photothermal Science and Techniques* (Chapman and Hall, London, 1996).

²A. Mandelis and P. Hess, *Progress in Photothermal and Photoacoustic Science and Technology: Life and Earth Sciences* (SPIE, Bellingham, WA, 1997), Vol. III.

³S. E. Bialkowski, in *Photothermal Spectroscopy Methods for Chemical Analysis*, edited by B. J. D. Winefordner (Wiley, New York, 1996).

⁴F. Garrido and A. Salazar, *J. Appl. Phys.* **95**, 140 (2004).

⁵A. Salazar, A. Sánchez-Lavega, A. Ocariz, J. Guitonny, G. C. Pandey, D. Fournier and A. C. Boccarda, *J. Appl. Phys.* **79**, 3984 (1996).

⁶A. Mandelis, S. B. Peralta and J. Thoen, *J. Appl. Phys.* **70**, 1761 (1991).

⁷R. Li Voti, G. L. Liakhov, S. Paoloni, C. Sibilila, and M. Bertolotti, *J. Optoelectron. Adv. Mater.* **3**, 779 (2001).

⁸J. F. Power, *Rev. Sci. Instrum.* **73**, 4057 (2002).

⁹J. Fivez and J. Thoen, *J. Appl. Phys.* **75**, 7696 (1994).

¹⁰C. Glorieux, J. Fivez, and J. Thoen, *J. Appl. Phys.* **73**, 684 (1993).

¹¹R. Li Voti, C. Sibilila, and M. Bertolotti, *Int. J. Thermophys.* **26**, 1833 (2005).

¹²M. H. Xu, J. C. Cheng, and S. Y. Zhang, *J. Phys. D: Appl. Phys.* **31**, 3154 (1998).

¹³Z.-J. Chen and S. Y. Zhang, *Chin. Phys. Lett.* **27**, 026502 (2010).

¹⁴R. Kolarov and T. Velinov, *J. Appl. Phys.* **83**, 1878 (1998).

¹⁵A. Salazar and R. Celorrio, *J. Appl. Phys.* **100**, 113535 (2006).

¹⁶J. Fivez and J. Thoen, *J. Appl. Phys.* **79**, 2225 (1996).

¹⁷T. T. N. Lan, U. Seidel, and H. G. Walther, *J. Appl. Phys.* **77**, 4739 (1995).

¹⁸U. Seidel, T. T. N. Lan, H. G. Walther, B. Schmitz, J. Geerkens, and G. Goch, *Opt. Eng.* **36**, 376 (1997).

¹⁹A. Mandelis, F. Funak, and M. Munidasa, *J. Appl. Phys.* **80**, 5570 (1996).

²⁰C. Glorieux, R. Li Voti, J. Thoen, M. Bertolotti, and C. Sibilila, *J. Appl. Phys.* **85**, 7059 (1999).

²¹Y. Cui, P. Xiao, and R. E. Imhof, *Int. J. Thermophys.* **26**, 213 (2005).

²²B. Su-Yuan, T. Zhen-An, H. Zheng-Xing, Y. Jun, and W. Jia-Qi, *Chin. Phys. Lett.* **25**, 593 (2008).

²³A. Mandelis, E. Schoubs, S. B. Paralta, and J. Thoen, *J. Appl. Phys.* **70**, 1771 (1991).

²⁴C. Glorieux, Z. Bozoki, J. Fivez, and J. Thoen, *J. Appl. Phys.* **78**, 3096 (1995).

²⁵T. T. N. Lan, U. Seidel, H. G. Walther, G. Goch, and B. Schmitz, *J. Appl.*

- Phys.* **78**, 4108 (1995).
- ²⁶R. Celorrio, A. Mendioroz, E. Apinaniz, A. Salazar, C. Wang, and A. Mandelis, *J. Appl. Phys.* **105**, 083517 (2009).
- ²⁷L. Liu, C. Wang, X. Yua, and A. Mandelis, *J. Appl. Phys.* **107**, 053503 (2010).
- ²⁸P. Martínez-Torres, A. Mandelis, and J. J. Alvarado-Gil, *J. Appl. Phys.* **106**, 114906 (2009).
- ²⁹M. A. Fromowitz, P. Yeh, and S. Yee, *J. Appl. Phys.* **48**, 209 (1977).
- ³⁰A. Harata and T. Sawada, *J. Appl. Phys.* **65**, 959 (1989).
- ³¹M. A. Schweitzer and J. F. Power, *Appl. Spectrosc.* **48**, 1054 (1994).
- ³²R. J. W. Hodgson, *J. Appl. Phys.* **76**, 7524 (1994).
- ³³J. C. Ciccone-Nogueira, M. C. Borsatto, W. C. Souza-Zaroni, R. Pereira Ramos, and R. G. Palma-Dibb, *J. Appl. Oral Sci.* **15**, 305 (2007).
- ³⁴K. M. Rode, P. M. de Freitas, P. R. Lloret, L. G. Powell, and M. L. Turbino, *Lasers Med. Sci.* **24**, 87 (2009).
- ³⁵S. Beun, T. Glorieux, J. Devaux, J. Vreven, and G. Leloup, *Dent. Mater.* **23**, 51 (2007).
- ³⁶M. Kawaguchi, T. Fukushima, and K. Miyazaki, *J. Dent. Res.* **73**, 516 (1994).
- ³⁷Y. K. Lee, *Dent. Mater.* **23**, 124 (2007).
- ³⁸N. Silikas, G. Eliades, and D. C. Watts, *Dent. Mater.* **16**, 292 (2000).
- ³⁹A. Mandelis, *J. Math. Phys.* **26**, 2676 (1985).
- ⁴⁰E. T. Whittaker and G. N. Watson, *A Course on Modern Analysis* (Cambridge University Press, Cambridge, 1934).
- ⁴¹L. Fabbri and F. Cernuschi, *J. Appl. Phys.* **82**, 5305 (1997).
- ⁴²H. Qu, C. H. Wang, X. Guo, and A. Mandelis, *J. Appl. Phys.* **104**, 113518 (2008).
- ⁴³L. G. P. Moraes, R. S. F. Rocha, L. M. Menegazzo, E. B. Araújo, K. Yukimitu, and J. C. S. Moraes, *J. Appl. Oral Sci.* **16**, 145 (2008).
- ⁴⁴C. Rahiotis, A. Kakaboura, M. Loukidis, and G. Vougiouklakis, *Eur. J. Oral Sci.* **112**, 89 (2004).
- ⁴⁵B. Williams and M. Braden, *J. Dent. Res.* **60**, 990 (1981).
- ⁴⁶A. Mandelis, *Diffusion-Wave Fields: Mathematical Methods and Green Functions* (Springer, New York, 2001), pp. 567–568.
- ⁴⁷W. H. Press, B. P. Flannery, S. A. Teukolsky, and W. T. Vetterling, *Numerical Recipes: The Art of Scientific Computing* (Cambridge University Press, Cambridge, 1986).
- ⁴⁸G. B. dos Santos, R. V. Monte Alto, H. R. Sampaio Filho, E. M. da Silva, and C. E. Fellows, *Dent. Mater.* **24**, 571 (2008).
- ⁴⁹A. Matvienko, A. Mandelis, and S. Abrams, *Appl. Opt.* **48**, 3192 (2009).
- ⁵⁰J. P. Fouassier, *Photoinitiation, Photopolymerization, and Photocuring* (Hanser Gardner, Cincinnati, OH, 1995).
- ⁵¹G. Odian, *Principles of Polymerization* (Wiley, New York, 1991).
- ⁵²C. Pianelli, J. Devaux, S. Bebelman, and G. Leloup, *J. Biomed. Mater. Res.* **48**, 675 (1999).
- ⁵³M. A. Zambrano-Arjona, R. Medina-Esquivel, and J. J. Alvarado-Gil, *J. Phys. D: Appl. Phys.* **40**, 6098 (2007).
- ⁵⁴S. Asmusen, G. Arenas, W. D. Cook, and C. Vallo, *Dent. Mater.* **25**, 1603 (2009).